Available online at www.sciencedirect.com
SCIENCE DIRECT®
International Journal of Mass Spectrometry 231 (2004) 51–58
International Journal of Mass Spectrometry
www.elsevier.com/locate/ijms

Initial velocity of secondary ions from *XY*-TOF technique, simultaneous calibration by residual gas ionization

T. Jalowy [a,*], Th. Weber [a], R. Dörner [a], L. Farenzena [b], V.M. Collado [b], E.F. da Silveira [b], H. Schmidt-Böcking [a], K.O. Groeneveld [a]

[a] *Institut für Kernphysik der J.W.Goethe Universität, August-Euler-Str. 6, D-60486 Frankfurt am Main D-60486, Germany*
[b] *Pontifícia Universidade Católica, Depto. de Física, CP 38071, 22452-970 Rio de Janeiro, Brazil*

Received 3 January 2003; accepted 4 September 2003

Abstract

A crucial parameter to distinguish the prompt secondary ion emission from surfaces after particle impact from the delayed one is $T_0(m/q)$, the time-of-flight (TOF) of ions with a given mass m and charge q "emitted" with zero velocity. This quantity is also an important reference for the measurement of prompt ion emission velocity distribution.

Presented is a novel and accurate method to determine $T_0(m/q)$, based on position sensitive *XY*-TOF analysis of residual gas ionization along the projectile trajectory, which is a low-pressure version of the traditional cloud chamber technique. Measurements using a mixture of He, Ne and Ar gases at low pressure (10^{-5} mbar) were performed to illustrate this new T_0-gas target calibration method. Secondary ion emission of H_n^+, $C_nH_n^+$ and Li^+ ions from C, Al and LiF targets, bombarded by MeV Ar^0 and N^0 projectiles, is analyzed. It is found that, in contrast to Li^+, hydrogen and hydrocarbon ions are always promptly emitted. The initial velocity distribution of H_2^+ is determined and discussed.

PACS: 34.50.Dy; 39.90+d

Keywords: Secondary ion desorption; Time-of-flight; Position sensitive detector; Initial velocity; *XY*-TOF

1. Introduction

In spite of decades of research [1–5], the understanding of ion desorption mechanisms is still a challenging problem. The two main reasons of this persisting interest is, on one hand, the richness—or complexity—of the interaction process between fast projectiles and solid matter and, on the other hand, the impressive evolution of data acquisition and data treatment systems providing access to more comprehensive information.

Basically, ion desorption is caused by energy or linear momentum transfer from the projectile to the target atoms. This transfer may occur in one collision or in multiple collisions with electrons or nuclei of the solid. If the recoiling electrons or nuclei do not escape "immediately" from the material (*prompt secondary emission*), they produce a cascade of further collisions or defects in the solid which eventually causes a *delayed secondary emission*. The time limit between prompt and delayed secondary emission processes is therefore qualitative and, for practical reasons, it is defined by the capability of experimental distinction (time resolution in this work is about 1 ns).

One of the main goals in performing initial velocity (v_0) measurements is the access to detailed information on ion emission mechanisms which, in turn, are related to projectile–solid interactions [6]. Time-of-flight (TOF) techniques offer a practical way to identify the emitted species (mass spectrometry), as well as to determine their desorption yields and axial (normal to the surface) velocities. The ions, emitted typically with less than 10 eV, are accelerated to keV energies in order to have efficient detection, to identify desorbed charged species by TOF according to the mass/charge (m/q) ratio and to measure their velocity distribution. Ions, with the same m/q ratio but different initial axial velocities, reach the detector at slightly different TOFs. For such a measurement, the spectrometer must

* Corresponding author. Tel.: +49-69-798-24291; fax: +49-69-798-24212.
E-mail address: jalowy@hsb.uni-frankfurt.de (T. Jalowy).

1387-3806/$ – see front matter © 2003 Elsevier B.V. All rights reserved.
doi:10.1016/j.ijms.2003.09.007

have sufficiently stable and homogeneous electric fields, so that the observed TOF differences are attributed only to the initial axial velocity distribution. The determination of radial velocities is necessary to acquire complete energy and angule distributions. Radial velocity measurements can be performed by extending the TOF system with a position sensitive *XY* detector.

The spectrometer described in this work is designed similarly to Cold Target Recoil Ion Momentum Spectroscopy (COLTRIMS) spectrometers [7] developed over the last 15 years. The parameters of the spectrometer (region lengths, target and grid potentials) should be known with sufficient accuracy to permit precise determination of v_0. The measurement of these parameters is not an easy task since high transmission grids are very fragile and allow field leakage which deteriorates the v_0 accuracy.

After a brief literature review of initial velocity analysis of secondary ions (SI), a new method for TOF calibration by residual gas ionization is presented.

2. The $T_0(m/q)$ calibration method for initial energy determination

The first SI initial energy measurements were done by Fürstenau et al. [8] in 1977. Becker [9], in 1982, analyzed TOF peak shapes by using two acceleration regions (double-grid method) and one drift region. The first region is characterized by an axial length of few millimeter as well by a weak field that broadens the mass peaks in order to reduce instabilities and uncertainties. The high field in the second acceleration region and the length of the drift region provide adequate ion optics and the minimum kinetic energy necessary for high SI detection efficiency and reasonable mass separation.

Macfarlane et al. [10] in 1987 observed energy shifts in the SI initial energy spectra for targets of different surface conduction properties. They attributed this effect to surface charging and also introduced the concept of delayed secondary emission: for secondary ions in the 0–0.2 ns range. The hypothesis of nuclear track charging was also discussed by Wien [11] and by the Uppsala Group [12,13]. The double-grid method has been employed in different configurations, e.g., with zero field in the first region by da Silveira et al. [14] in 1989 to compare TOF peak shapes of positive and negative secondary ions.

The basic challenge of these methods is to determine precisely the quantity $T_0(m/q)$, defined—for a given spectrometer—as the absolute TOF value for ions with mass m and charge q that are emitted with $v_0 \approx 0$. Wien et al. [15], operating a ^{252}Cf-PDMS spectrometer with two acceleration regions, improved the technique of measuring accurate absolute TOFs; they employed grid-line references produced by SI desorption induced by the projectiles on the grids. This method was later used, e.g., by de Castro et al. [16].

In the current work, we have used a new strategy to reliably calibrate the $T_0(m/q)$ on-line. The spectrometer [17], equipped with a position sensitive detector, is set up with a relatively long first acceleration region (order of 10 cm). This allows a variation of the projectile–target–impact-angle θ_p in between the accessible range with 100% transmission and a longer trajectory of the projectile inside the acceleration region. This permits the employment of a novel technique for measuring $T_0(m/q)$, based on the residual gas ionization along the projectile track inside the spectrometer.

A mixture of noble gases (with average $v_0 \approx 0$ ions) is introduced into the chamber to enhance the ionization rate along the primary projectile's trajectory for simultaneous acquisition of TOF spectra from solid and gas targets (Fig. 1). It is then possible to determine the $T_0(m/q)$ of gas ions originating along the projectile's trajectory, including in particular the position of impact on the solid target surface. The technique is sensitive enough to detect charging effects for SI emission on insulating surfaces and can be seen as an up-dated version of a cloud chamber.

Fig. 1 illustrates schematically the particle trajectories inside the scattering chamber. The circular form of the detector in the picture contains a measured *XY* distribution of the ions. This distribution is characterized by the projection of the primary beam's trajectory inside the spectrometer and by a central "image" of the target spot. The beam spot on a solid target has roughly the spatial resolution of the detector (about 0.1 mm diameter) which is negligible compared to the detector diameter (50 mm). Residual gas ionization takes place all along the beam trajectory. The gas ions (which are produced with a mean initial velocity much smaller than the solid target ions) are accelerated towards the detector in a uniform electric field.

Fig. 2 displays the spectrometer configuration. *XZ* is the plane of incidence and *Z* is the symmetry axis; a grid parallel to the target and to the detector provides two acceleration regions, with electric fields equal to $\varepsilon_1 = (U_1 - U_2)/d_1$ and $\varepsilon_2 = U_2/d_2$ respectively, U_1 and U_2 being the voltages applied on the target and on the grid. The projectiles, whose direction is given by the angle θ_p, with respect to the target normal, induce (i) desorption at the target surface site located at coordinates $x = y = z = 0$ and (ii) residual gas ionization along the z_p, x_p ($=z_p\mathrm{tg}(\theta_p)$), y_p ($=0$) trajectory. The TOF start signal is produced by secondary electrons (SE) leaving the target from the rear surface. They are accelerated towards a microchannel plate detector by a electric field much higher than the their initial energy distribution to provide a precise time reference and are detected at the time Δt_e after the projectile–target impact.

The TOF stop signals are delivered by the detection of secondary ions at points defined by coordinates x, y and $z = d_1 + d_2$, on the position sensitive detector, and at the TOF $t_1 + t_2$ (see Fig. 2). The measured clock time interval t, between stop and start signal is $t = T - \Delta t_e + t_{delay}$, where t_{delay} is an extra delay time due to electronics and $T = t_1 + t_2$ is the TOF for secondary ions. Defining v_p as the projectile

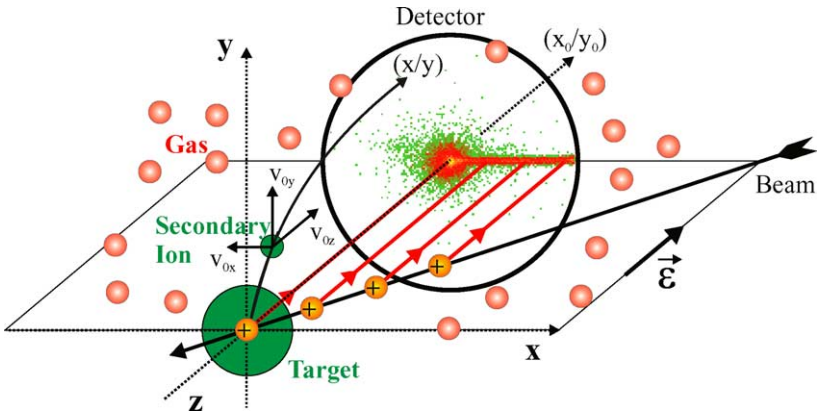

Fig. 1. Schematic of the analyzing chamber geometry. *Y* is the vertical axis. The beam is horizontal, enters into the chamber towards negative *x* and *z* coordinates and hits the solid target surface at $x = y = z = 0$. Residual gas atoms are ionized along the beam trajectory and are accelerated towards the detector, their registration occurs along the *x* direction.

velocity, the ionization of a given gas molecule happens at time $t_p = x_p/(v_p \sin\theta_p)$ before the projectile impacts on the solid target, which occurs at $T = 0$. So that for gas molecules the TOF is $T_{gas} = t_1 + t_2 - t_p$.

Using these considerations, the TOF of $v_0 = 0$ ions can be written as [18,19].

$$T = \sqrt{\frac{2m}{q}}\left[\frac{d_1 - x\,\mathrm{cotg}(\theta_p)}{\sqrt{(U_1-U_2)(1-x/d_1\,\mathrm{cotg}(\theta_p))}} + \frac{d_2}{\sqrt{(U_1-U_2)(1-x/d_1\,\mathrm{cotg}(\theta_p))}+\sqrt{(U_1-U_2)(1-x/d_1\,\mathrm{cotg}(\theta_p))+U_2}}\right] - \frac{x}{v_p\sin(\theta_p)} \quad (1)$$

where $T = T_{gas}$ and $x = x_p$ for gas ions; $x = 0$ for target ions. This equation allows also a connection between *T* and *z* values, for a given ion.

For $v_0 > 0$, a secondary ion may leave the solid in any direction defined by both the polar angle θ (with the *Z*-axis) and the azimuth angle φ (angle of the ion trajectory projection, on the *XY* plane, with the *X*-axis). The initial energy of secondary ions being $E_0 = mv_0^2/2$, its "axial" energy is $E_{0z} = mv_{0z}^2/2 = E_0\cos^2\theta$.

To precise definitions: *XY*-plot displays the number of ion impacts as a function of the coordinates *X* and *Y* on the detector; *XT* (or *YT*) plot displays the number of ion impacts as a function of arrival position *X* (or *Y*) and TOF. The *XY*-TOF data (analyzed through the plots *XY*, *XT* and *YT*) provides basic information for accurate calibration of the time and position: (i) the *X*-axis can be easily determined by the projection of the primary beam's trajectory in the gas, (ii) the *Z*-axis is found by reflection symmetry with respect to the *X*-axis and by the smallest *x* value of the oblique lines on the plot *x* position versus TOF ("*XT*-oblique line,"

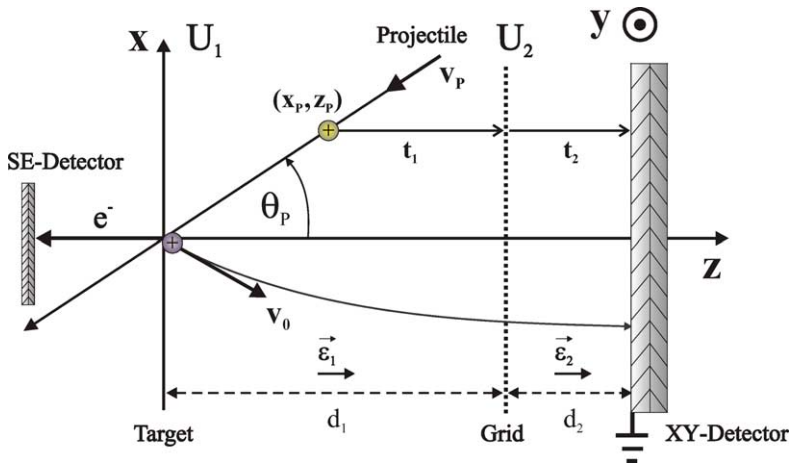

Fig. 2. The ion dynamics in the horizontal *XZ* plane. The beam impinges on the target at the polar angle θ_p. The electric field is axial in the region defined by the target and the detector surface, changing intensity at the grid. Gas ions are produced with negligible initial velocity and accelerated in the *z* direction onto the detector. Secondary ions are emitted with parabolic trajectories from the target with initial velocity v_0. The measurement of their TOF and impact coordinates on the detector allows the determination of the angle and velocity distribution of the secondary ion emission.

corresponding to the residual gas ionization events), (iii) the T_0 determination by the interception of the gas XT-oblique line with the T-axis.

For the energy and angule distributions of the emitted ions, it is extremely important to have the correct calibration of the TOF spectrometer, which means: (i) to guarantee that the collision time of each impact takes place accurately at $T = 0$ and at the coordinates $x = y = 0$, (ii) to know the parametric values of the function $T_0(m/q)$. This problem is partially solved by using the same secondary ion detector for detecting the UV radiation emitted promptly after impact: these photons generate a narrow TOF peak at time $T_{ph} = (d_1 + d_2)/c$.

A further improvement is gained by introducing a mixture of noble gases (70% He, 15% Ne and 15% Ar at 10^{-5} mbar) to enhance the ionization rate and thereby the beam image on the detector. This procedure makes it possible not only to determine the $x = y = 0$ point on the XY-plot, but even more importantly, also to provide many $T_0(m/q)$ values necessary for the accurate TOF calibration in the XT-plot. The use of monoatomic gases helps to preserve $v_0 \approx 0$ and avoid spreading out the beam image, either: (i) by elimination of the molecular Coulomb explosion and producing narrow XT-oblique lines, and (ii) by greatly decreasing of their adsorption on the solid target, producing a clear end point of these lines. In contrast to ions formed at solid surfaces, those produced from low-pressure gases have almost zero average initial velocity. Thermal energy is about 3/2 $k_B T_G = 38$ meV (at room temperature, $T_G \approx 300$ K), and typically the recoiling energy of a He ion is 2 meV after ionization by fast projectiles [20]. The noble gases are therefore very well suited for time calibration.

From Eq. (1) it can be shown that, in first order approximation ($x \ll d_1$ and $d_2 \ll d_1$), the relationship between the x position of a detected residual gas ion and the time of its detection, T_{gas}, is:

$$x = \sqrt{\frac{q(U_1 - U_2)}{2m}}[T_0(m/q) - T_{gas}]\mathrm{tg}(\theta_p) \quad (2)$$

where $T_0(m/q)$ is the TOF sought for the solid target secondary ions with $v_0 = 0$:

$$T_0(m/q) \approx d_1\sqrt{\frac{2m}{q(U_1 - U_2)}} \quad (3)$$

Eq. (2) also shows that the slope dx/dT of the oblique lines in the XT-plot is directly proportional to tg(θ_p), which turns out to be a convenient method to determine the primary projectile's incidence angle [21].

In general, conventional spectrometers have $d_1 \ll d_2$ (instead of the above approximation $d_1 \gg d_2$) and should generate quite short XT-oblique lines. In spite of this fact, ions should be produced and accelerated in the gas close to region $x \approx y \approx z \approx 0$, which is the most important region for the $T_0(m/q)$ fitting procedures.

3. Results

Fig. 3 shows the x position plotted versus TOF (the XT-plot) of ions produced when an Al film (200 nm thick)

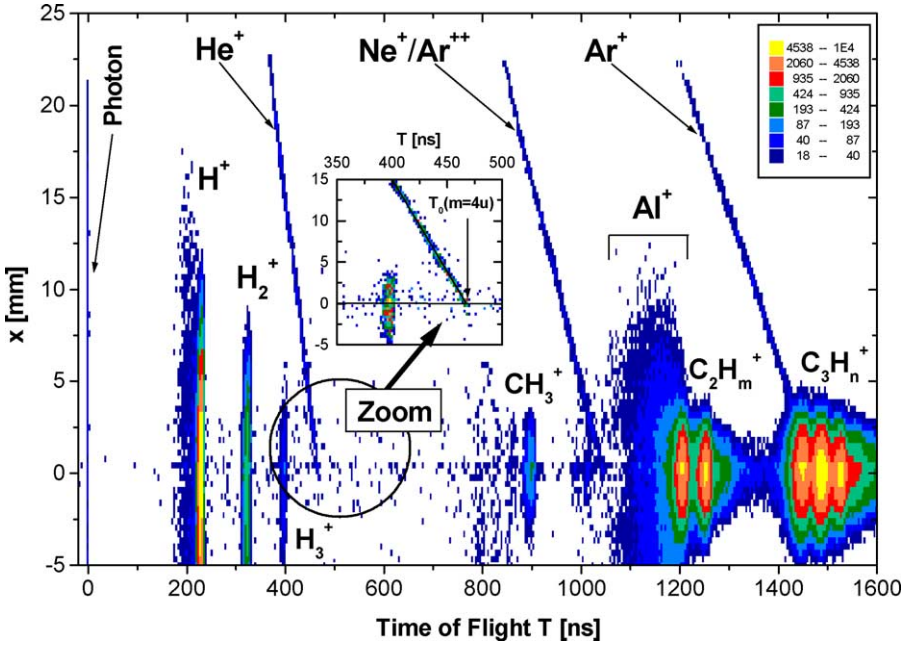

Fig. 3. A typical XT-plot, representing the x-coordinate of ion impact on the detector plotted vs. the corresponding TOF T. The argon beam is ionizing a He/Ne/Ar gas mixture and produces secondary ions at the Al foil surface. The oblique lines at positive x are due to the gas ion detection. The line perpendicular to the T-axis at $T = 0$ is generated by photons emitted from the bombarded target. The other structures are due to secondary ions desorbed from the solid target surface. The important points are the intersections at $x = 0$ between the oblique lines and the T-axis: they give the T_0 values for gas ions emitted very close of the aluminum solid target.

is bombarded by 25 keV/u neutral argon atoms, under an incidence angle of $\theta_p = 37^\circ$. Electric potentials of the spectrometer are $U_1 = 2.970$ kV (±0.2%) and $U_2 = 0.040$ kV (±1.3%); the region lengths were determined from this *XT*-plot as being $d_1 = 84.1$ mm (±0.2%) and $d_2 = 7.0$ mm (±2.9%).

The peaks centered at $x = 0$ are due to secondary ions coming from the solid target surface, while the positive-x oblique lines are due to gas atoms and molecules ionized along the beam trajectory. A narrow peak (about 1 ns width) is visible close to the TOF origin ($T_{ph} = 0.3$ ns). This peak is caused by UV radiation, emitted by the target under projectile impact, arriving everywhere on the *XY* detector. The hydrogen and hydrocarbon ion peaks are due to adsorbates on the Al_2O_3 surface layer. The peaks show some asymmetry around $x = 0$, indicating that the beam direction plays a role in the desorption phenomenon (e.g. [22,23]). The hydrogen ion group (H^+, H_2^+ and H_3^+) and the CH_3^+, $C_2H_3^+$, $C_2H_5^+$, $C_3H_n^+$ ($n = 3, 4, 5$) peaks dominate the spectrum. The Al^+ peak is also intense, but rather broad in position and TOF due to emission with high axial and radial v_0. In general, it is difficult to distinguish the Al^+ peak from the $C_2H_3^+$ peak (both have $m/q \approx 27$ u/e); however, by using the *XY*-TOF method, the contribution of each species can be determined as shown in Fig. 3: the Al^+ and the $C_2H_3^+$ ions are represented by black and gray areas, respectively. Jalowy et al. [24] have shown recently that indeed high velocity surface secondary ions are emitted in a direction perpendicular to the incident beam.

The oblique lines are produced by He, Ne and Ar atoms ionized by beam–gas collisions. When multiple charge states of the gas ions are populated, they give rise to several m/q oblique lines. In the case of Fig. 3, only three lines are visible. The magnification of the He^+ line diving into the *T*-axis clearly shows how $T_0(m/q = 4)$ can be determined. Note that the approximation of Eq. (3), the coefficient $d_1/(U_1 - U_2)^{1/2}$ can be directly determined from a T_0 data set. Starting from the nominal values U_1 and U_2 of the spectrometer parameters and using a initial value of d_1 given by this coefficient, a fitting procedure is applied to get more precise values of d_1 and d_2. Finally, including all the oblique lines of He, Ne and Ar, the best values of the parameters d_1, d_2, U_1, U_2 and θ_p are obtained, resulting in an independent and accurate calibration for the secondary ion TOFs. In such a spectrometer configuration, the TOF's of 0.0 and 0.1 eV Ar^+ secondary ions are predicted to be 1473.4 and 1465.2 ns, respectively. The calibration accuracy is typically of the order of 1 ns.

A practical procedure and rigorous test of this TOF calibration by gas ions is the reduced TOF plot T_{red} [19]. From Eq. (1), one sees that the quantity $T_{red} = (q/2m)^{1/2}T + x/v_p \sin\theta_p$ does not depend on m/q, so that—if the values of the spectrometer parameters are correctly introduced in the equation—all the oblique lines shown in Fig. 3 must be transformed into just one line. The transformed data of the three gases overlap perfectly, as shown in Fig. 4. The solid line is a fit performed with Eq. (1). Small discrepancies between the fit and experimental data are attributed to field distortions close to the detector border ($x \approx 25$ mm). In order to have a more precise calibration close to $x = 0$, the

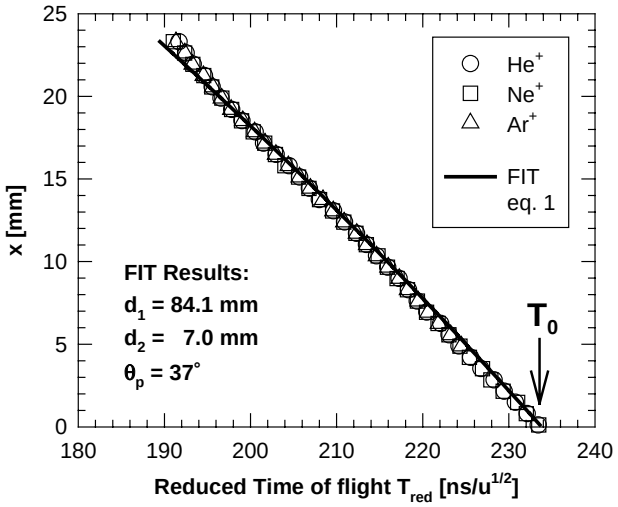

Fig. 4. Reduced TOF plot for He, Ne and Ar gas ions. For $v_0 = 0$ ions, TOF increases with $m^{1/2}$, so that $T_{red} \equiv T/m^{1/2} + x/v_p \sin\theta_p$ is mass independent for each x. The collapse of the transformed oblique lines into just one line demonstrates that the system is well calibrated, so that the T_0 function can be well determined for all the species desorbed from the solid target. The original noble gas data are the same as in Fig. 3.

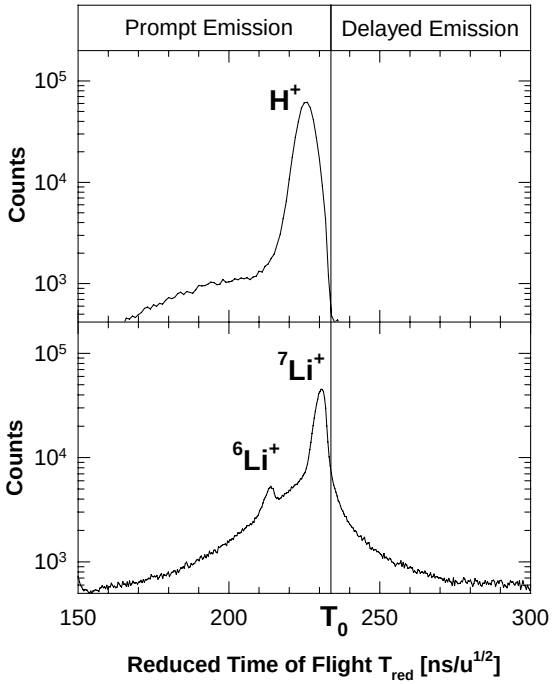

Fig. 5. Reduced TOF plot for H^+ and Li^+ secondary ions. The LiF target is bombarded by a 25 keV/u Ar^0 beam. The obtained T_0 value for H^+ ions is higher than their TOF distribution, showing that prompt emission occurs (top). In contrast, similar data for Li^+ ions show that T_0 falls inside the distribution (bottom). As negative v_0 values are not allowed for solid targets, the conclusion is that delayed emission does occur up to 40 ns after impact.

data corresponding to large x (e.g. $x > 15$ mm) should be eliminated from the fitting.

The reduced TOF calibration obtained as described above was used for other targets. In Fig. 5, it is used to compared the reduced TOF distributions of the H^+ and Li^+ secondary ions emitted by a LiF target. We clearly see that all of the H^+ ions are emitted prompt while all of the Li^+ ions are not. The accuracy of our calibration yields a reliable demonstration of delayed emission of Li^+ ions. Appreciable number of Li^+ ions are desorbed as late as 40 ns after the projectile impact, a value two orders of magnitude higher than the ones previous reported [10]. A possible mechanism responsible for such delay is the diffusion of bulk excitons up to the LiF surface [25]. The current results provide experimental data to test model predictions.

Other experimental data, acquired with a different extraction voltage ($U_1 = 3.000$ kV and $U_2 = 0.040$ kV), are presented in Fig. 6. Two targets, a carbon foil (50 nm) and a LiF (20 nm) layer evaporated onto another C foil (50 nm), were bombarded by 143 keV/u neutral nitrogen atoms ($\theta_p \approx 36^\circ$).

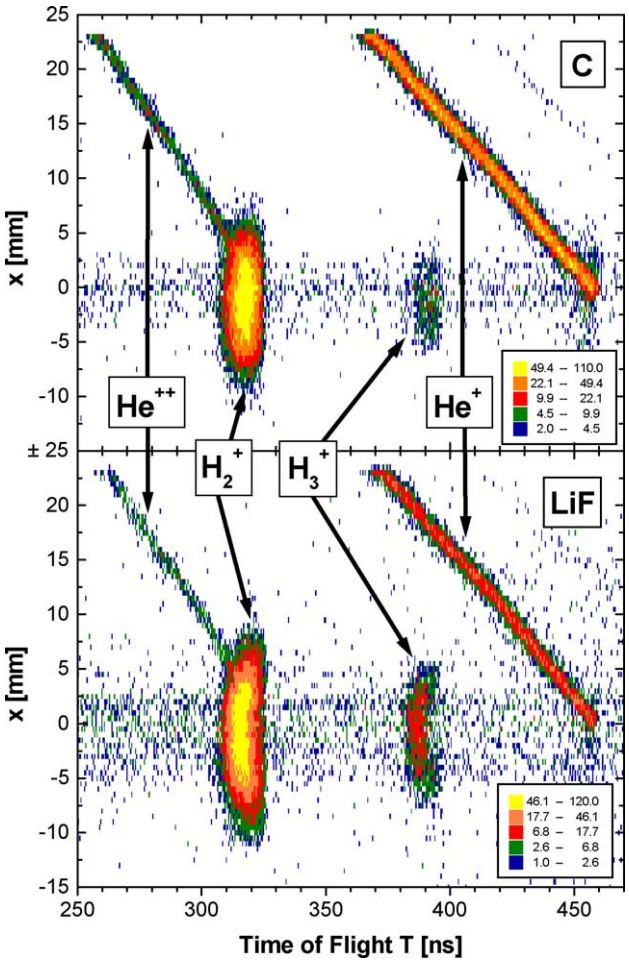

Fig. 6. Similar picture as Fig. 3, but here carbon target results (top) are compared with LiF target results (bottom). The He^{2+} gas atomic ions have the same m/q ratio as $H_2{}^+$ secondary ion molecules and, therefore, have the same T_0. Such measurement shows that (i) no $H_2{}^+$ ion is delayed emitted and (ii) their v_0 distribution is higher for LiF than for C targets.

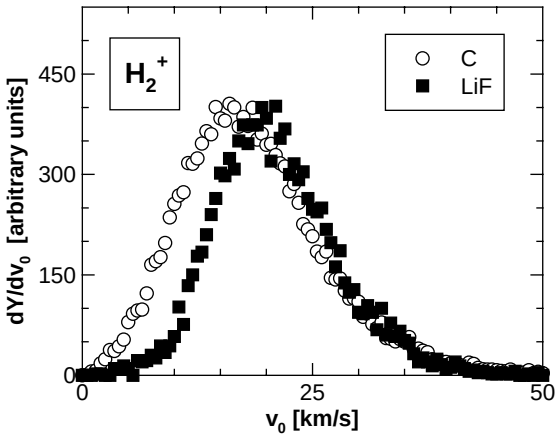

Fig. 7. The initial velocity distribution of $H_2{}^+$ ions from a carbon (○) and a LiF (■) target. The data are the same as in Fig. 6, but the distributions are normalized to the common maximum. The observed difference in the velocity of emission is due to charging up effects in the target surface.

The two oblique lines in Fig. 6 correspond to He^{2+} and He^+ gas ions, respectively, while the distributions centered on $x = 0$ are due to $H_2{}^+$ and $H_3{}^+$ ions emitted from the target surface. One sees that: (i) all the $H_2{}^+$ ions have a TOF shorter than $T_0(m/q = 2)$ and (ii) the $H_2{}^+$ TOF distributions are different for the C (conductor) and for the LiF (insulator) targets. Fig. 7 shows the $H_2{}^+$ total velocity distribution for the C and the LiF target. While there is no obvious difference for high velocity secondary ions ($v_0 > 25$ km/s), the low velocity ones are very sensitive to the electrical target properties. Such results are crucial for the determination of the ion desorption mechanism.

4. Discussion

The time interval for ion desorption after fast ion impact depends on several factors, for example: the time it takes for electrons to neutralize the track, the time it takes for the track region to cool down, and the time it takes for bulk secondary particles or electron excitations (e.g. excitons) to reach the surface. If the electric conductivity of the solid is high, like in metal targets, the energy transferred from the projectile to electrons is quickly dissipated and neutralization is fast (on the order of the inverse of plasma frequency). Therefore, emission of the metallic material occurs essentially by nuclear sputtering while ion emission of adsorbed contaminants (hydrogen, water, alkaline halide salts and hydrocarbons) are expected to occur also by electronic sputtering. No craters are formed on conductors unless the stopping power is very high [26]. If the target is an insulator, craters are likely to be formed, as well defects in the crystalline structure. The high temperature around the impact point creates new chemical species that may desorb as ions [27].

Fast projectiles ($v_p > 0.1 v_B$) cross each atomic layer of the target in less than picosecond time interval. If a recoiling

atom leaving the solid is produced by a projectile–nucleus collision in a layer not far from the surface the secondary ion emission process is necessarily "prompt." For insulators, the projectile ionizes the region near its trajectory and the time that secondary electrons need to return and neutralize the track is expected to be orders of magnitude higher than for conductors [15]. During this time period, the huge electrostatic potential energy created by the electron emission decreases and is partially transformed into kinetic energy of the particles (neutrals and ions) inside the track near the surface where the sputtering process takes place. For conductors, the track is neutralized fast, but the adsorbed excited molecules may stay ionized for a longer period, during which some of them dissociate. One method for verifying such a mechanism is measuring emission energies or angular distributions and comparing them with Coulomb explosion in gaseous targets [14].

The scenario described above is supported by the findings shown in the Figs. 6 and 7. The results presented in Fig. 6 lead to the following conclusions: (i) there is prompt emission of the H_2^+ ions, since they arrive at the detector before the He^{2+} ions emitted with average $v_0 = 0$; (ii) the initial velocity distributions of H_2^+ ions are different for the two targets, due to surface charging effects caused by the projectile; (iii) the surface charging does not show visible influence on the gas ions due to a cumulative charging effect, allowing the use of the obtained calibration for other targets. Coulomb explosion should not be the mechanism for H_2^+ emission, since these species are not atomic ions and H_2 clusters are not likely to exist under the present experimental conditions. Note that the H_2^+ and the H_3^+ *XT* distributions are slightly asymmetric with respect to the *T* (or *Z*) axis, which may be interpreted as an emission due to electronic excitations (typically symmetric) but disturbed by an oblique and charged projectile track [28,29]. It is also observed that, for both distributions, the charged insulator substrate does not allow low velocity emission. Therefore, the emission mechanism seems to be molecular ionization by the projectile (or H^+ attachment for the H_3^+), followed by repulsion due to a charged surface. Similar conclusion can be drawn from Fig. 7, in which it the total velocity distribution is plotted. This is possible only since the employed *XY*-TOF technique allows simultaneous determination of both radial and axial velocities.

5. Conclusions

Results of secondary ion velocity measurements are presented by using a position sensitive detector combined with a TOF technique (*XY*-TOF method). Because both axial and radial velocity distributions can be determined by this method, total velocity, energy and angular distributions can also be deduced. A special difficulty of such a method is the accuracy of low velocity measurements, which are extremely sensitive to spectrometer's parametric values.

In this work, a new method is described to perform very precise TOF calibration of desorbed ions by using simultaneous residual gas *XY*-TOF measurements. Analysis shows that the data obtained are indeed consistent and reliable. The basic idea of this method is applicable to similar spectrometers. As an example, H_2^+ initial velocity distribution data are presented for ions emitted from carbon and LiF targets, showing that values for low velocity ions are quite different for the two surfaces conductivities.

The T_0-gas method is particularly useful for unambiguously measuring times of delayed emission processes. We find clear evidence for delayed emission of Li^+ secondary ions in contrast to prompt emission of H^+ ions.

Acknowledgements

We gratefully acknowledge the support of this collaborative work by DAAD-Bonn, VW-Stiftung, Willkomm-Stiftung-Frankfurt a.M. (Germany), CAPES-PROBRAL and FAPERJ (Brazil). DFG and BMBF are also acknowledged for their partial support.

References

[1] P. Sigmund, Lectures on Collision Theory, Report Fysik Institut, Odense University, 1972.
[2] B. Sundqvist, R.D. Macfarlane, in: M.L. Gross (Ed.), Mass Spectrometry Reviews, vol. 4, John Wiley & Sons, 1985, p. 421.
[3] Y. Le Beyec, in: A.C.A. Souza, E.F. da Silveira, J.C. Nogueira, M.A.C. Nascimento, D.P. Almeida (Eds.), Review: Ion Desorption Phenomena Induced by Various Types of Multiple Charged Projectiles and by Photons on Solid Surfaces, Collision Processes of Ion, Positron, Electron and Photon Beams with Matter, World Scientific, 1992, p. 15.
[4] J.A.M. Pereira, E.F. da Silveira, Phys. Rev. Lett. 84 (2000) 5904.
[5] A. Brunelle, S. Della-Negra, J. Depauw, D. Jacquet, Y. Le Beyec, M. Pautrat, K. Baudin, H.H. Andersen, Phys. Rev. A 63 (2001) 22902.
[6] G. Betz, K. Wien, Int. J. Mass Spec. Ion Proc. 140 (1994) 1.
[7] R. Dörner, V. Mergel, O. Jagutzki, L. Spielberger, J. Ullrich, R. Moshammer, H. Schmidt-Böcking, Phys. Rep. 330 (2/3) (2000) 96.
[8] N. Fürstenau, W. Knippelberg, F.R. Krueger, G. Weiss, K. Wien, Z. Naturforsch 32a (1977) 711.
[9] O. Becker, Nucl. Inst. Methods 198 (1982) 53.
[10] R.D. Macfarlane, J.C. Hill, D. Jacobs, J. Trace, Microprobe Tech. 4 (1986–1987) 281.
[11] K. Wien, Radiat. Eff. Def. Solids 109 (1989) 137.
[12] S. Widdiyasekera, P. Hakånsson, B. Sundqvist, Nucl. Inst. Methods B 33 (1988) 836.
[13] D. Fenÿo, P. Hakånnson, B. Sundqvist, Nucl. Inst. Methods B 84 (1994) 31.
[14] E.F. da Silveira, M.G. Blain, E.A. Schweikert, J. Phys. 2 (1989) C2.
[15] K. Wien, Ch. Koch, N. van Tan, Nucl. Inst. Methods Phys. B 100 (1995) 322.
[16] C.C. de Castro, I.S. Bitensky, E.F. da Silveira, M. Most, K. Wien, Int. J. Mass Spectrom. Ion Process. 173 (1998) 1.
[17] T. Jalowy, R. Neugebauer, M. Hattass, J. Fiol, F. Afaneh, J.A.M. Pereira, E.F. da Silveira, H. Schmidt-Böcking, K.O. Groeneveld, Nucl. Inst. Methods Phys. Res. Sect. B 193 (2002) 792.

[18] T. Jalowy, R. Neugebauer, K.O. Groeneveld, C.R. Ponciano, L.S. Farenzena, E.F. da Silveira, Int. J. Mass Spectrom. 219 (2002) 343.
[19] T. Jalowy, R. Neugebauer, K.O. Groeneveld, C.R. Ponciano, L.S. Farenzena, E.F. da Silveira, Rev. Sci. Instrum. 73 (2002) 3187.
[20] M.A. Abdallah, C.R. Vane, C.C. Havener, D.R. Scultz, H.F. Krause, N. Jones, S. Datz, Phys. Rev. Lett. 85 (2000) 278.
[21] T. Jalowy, Dissertation, Institut für Kernphysik, der J.W. Goethe-Universität Frankfurt a.M., 2002. http://hsbpc1.ikf.physik.uni-frankfurt.de/publications/Diplom_Doktor_year.html
[22] R.M. Papaléo, G. Brinkmalm, D. Fenÿo, J. Eriksson, H.-F. Kammer, P. Demirev, P. Hakånnson, B. Sundqvist, Nucl. Inst. Methods B 91 (1994) 667.
[23] W. Ens, B.U.R. Sundqvist, A. Hedin, P. Hakånnson, G. Jonsson, Phys. Rev. B 39 (1989) 763.
[24] T. Jalowy, R. Neugebauer, L.S. Farenzena, V.M. Collado, H. Schmidt-Böcking, E.F. da Silveira, K.O. Groeneveld, AIP Conf. Proc. 680 (2003) 176.
[25] J.A.M. Pereira, E.F. da Silveira, Surf. Sci. 390 (1997) 158.
[26] J. Henry, A. Barbu, B. Leridon, D. Lesueur, A. Dunlop, Nucl. Inst. Methods Phys. Res. Sect. B 67 (1992) 390.
[27] R.M. Papaléo, P.A. Demirev, J. Eriksson, P. Hakånnson, B.U.R. Sundqvist, Int. J. Mass Spectrom. Ion Proc. 152 (1996) 193.
[28] M. Most, K. Wien, A. Brunelle, S. Della Negra, J. Depauw, D. Jacquet, M. Pautrat, Y. LeBeyec, Nucl. Inst. Methods Phys. Res. Sect. B 164/165 (2000) 772.
[29] M. Most, K. Wien, A. Brunelle, S. Della Negra, J. Depauw, D. Jacquet, M. Pautrat, Y. LeBeyec, Nucl. Inst. Methods Phys. Res. Sect. B 168 (2000) 203.